Research Article | Vol. 30, No. 24 / 21 Nov 2022 / Optics Express 43417
Optics EXPRESS

Terahertz radiation detection with a cantilever-based photoacoustic sensor

Sucheta Sharma,[1,*] Mohsen Ahmadi,[2] Jussi Rossi,[3] Markku Vainio,[3,4] Zhipei Sun,[2] Andreas Steiger,[5] and Erkki Ikonen[1,6]

[1]Metrology Research Institute, Aalto University, Espoo, Finland
[2]Department of Electronics and Nanoengineering, Aalto University, Espoo, Finland
[3]Photonics Laboratory, Tampere University, Tampere, Finland
[4]Department of Chemistry, University of Helsinki, Helsinki, Finland
[5]Physikalisch-Technische Bundesanstalt (PTB), Berlin, Germany
[6]VTT MIKES Metrology, Espoo, Finland
[*]sucheta.sharma@aalto.fi

Abstract: We report the photoacoustic (PA) response in the terahertz (THz) range by employing a detection process actuated with a silicon cantilever pressure sensor and a carbon-based radiation absorber. The detection relies on the mechanical response of the cantilever, when the volume of the carrier gas inside the PA cell expands with the heat produced by the radiation absorber. The detector interferometrically monitors the movement of the cantilever sensor to generate the PA signal. We selected the absorber material with the highest THz responsivity for detailed studies at 1.4 THz (214 µm wavelength). The observed responsivities of two different radiation absorbers are nearly the same at 1.4 THz and agree within 10% with responsivity values at 0.633 µm wavelength. The results demonstrate the potential of covering with a single PA detector a broad spectral range with approximately constant responsivity, large dynamic range, and high damage threshold.

1. Introduction

The terahertz (THz) gap has been an important research topic over the last few decades to discover robust, controllable, and novel technological possibilities for the generation and detection of THz radiation [1–4]. The THz spectral range includes the region spanning from 0.1 to 10 THz (~ 3000 µm to 30 µm in wavelength) and has enormous potential for different real-world applications including toxic chemical detection, industrial process control, medical imaging, spectroscopic studies, security applications and explosive material detection [1–7]. Research efforts in the field have resulted in innovative solutions to contribute to the development of technologies that include thermal, optical, and semiconductor-based detection processes [1–3,8,;9]. Recent studies have shown the potential of optomechanical detection systems [10–12]. A silicon cantilever-based sensor for molecular spectroscopy applications in the THz range has been demonstrated [12]. For mechanically responsive thermal detection processes, Golay cells serve as excellent detectors and with proper window materials the technology can be applied not only in the THz, but a considerably large spectral range can be covered from ultraviolet (UV) to millimeter (mm) wavelengths [1].

The membrane-based pressure sensing method, as used in Golay cells, often has a restriction on the highest detectable power as the developed stress due to the gaseous pressure can cause mechanical damage to the membrane. As examples, we can mention two commercial devices which have highest permissible power level at 10 µW [13] and at 500 µW [14]. In some

#469295 https://doi.org/10.1364/OE.469295
Journal © 2022 Received 4 Jul 2022; revised 23 Sep 2022; accepted 23 Sep 2022; published 10 Nov 2022

Optics EXPRESS

applications, however, a detection method with a large dynamic range and high damage threshold is required to avoid the need of multiple detection schemes for different power level ranges. Furthermore, a Golay cell detector may have nonuniform spatial responsivity for a THz laser beam, because of the detector structure to optimize the signal strength [13].

In our previous studies, we reported a robust silicon cantilever-based pressure sensor for photoacoustic (PA) detection from UV to Infrared (IR) region [15–17], which is a promising candidate also for THz detection. The window transmittance is a key parameter for the detection process to extend the spectral sensitivity towards the THz range. Apart from that, the sensing process of the detector highly depends on the radiation absorber material [15] and the pressure sensor of suitable dimensions. A linear dynamic range of nearly six orders of magnitude can be achieved with PA detection [16], extending the detectable power range from nanowatt level to several milliwatts, or even up to 600 mW [17]. The absorber was damaged at power levels above 1 W. However, the cantilever mechanics would sustain vibration amplitudes corresponding to power levels well above 1 W if there would be a more robust absorber material with similar responsivity.

This article presents a PA detection method for THz radiation, employing the silicon cantilever-based pressure sensor. The main motivation involves not only the THz detection but also understanding and comparing the detector responses of different absorber materials in the visible and THz region. We determined good spatial uniformity of responsivity over an area of 3 mm in diameter when probed with a THz laser beam of 1.9 mm full width at half maximum. We also studied the effect of different chopping frequencies of the THz radiation on the PA response. The highest THz power used in the experiments was 11 mW. Furthermore, the responsivity of the absorber which produced better PA signal in the THz, was compared at 0.633 μm and 214 μm (i.e., 1.4 THz) wavelengths. The information on responsivity is essential for the evaluation of the overall performance of the detector, to function with broad spectral sensitivity covering UV to THz range. The following sections contain descriptions of the experimental arrangements with results and analysis.

2. Experimental

2.1. Photoacoustic detector

The main parts of the PA detector are the radiation absorber, pressure sensor and entrance window. For the four absorber sample types studied in [15], Vantablack and Nextel show almost an order of magnitude lower responsivity at 0.633–15 μm range than candle soot and S-VIS samples. Although the responsivity of our Vantablack absorbers could be improved with thicker coating [18], we selected our available absorbers with higher UV-IR responsivity for further studies in the THz range: candle soot produced at the tip of a flame and commercially available spray applied coating of randomly oriented carbon nanotube (CNT) surface, i.e., S-VIS samples of same specifications as reported in [15]. As a radiation absorber material, candle soot shows better signal strength and therefore has higher detection responsivity than CNT from UV to IR region [15,17], but the responsivity of soot material decreases as the incident radiation wavelength increases, while that of CNT stays approximately constant. Furthermore, both absorber materials show reasonably uniform spatial responsivity [15]. Polarization effects are not expected with the candle soot and CNT absorbers (i.e., S-VIS), because both materials appear random in scanning electron microscope pictures [15].

The main component of the pressure sensor is micromechanically produced silicon cantilever. The chosen cantilever dimensions in this work are in accordance with our previous analysis [16]. The aim is not about testing the detection linearity in the THz range as the linear behavior of the detector, in this case, is not expected to differ from the results of our previous studies which were carried out at shorter wavelengths [16,17]. The window transmittance of the detector plays an important role in estimating absorber responsivity at different wavelengths. For the present

Optics EXPRESS

experiments, the window material was changed to Polymethylpentene (TPX) [13] from Potassium Bromide (KBr), where the latter was employed in our studies from UV to IR range [15–17].

2.2. Generation and detection of THz radiation

Figure 1 illustrates the experimental process of THz radiation generation and detection with a terahertz time-domain spectroscopy (THz-TDS) setup. Femtosecond pulses at 800 nm from a mode-locked Ti: sapphire laser with 75 MHz repetition rate were directed to low-temperature Gallium arsenide (LT-GaAs) photoconductive antennas. Two main processes give rise to THz radiation in photoconductive antennas: photocarrier generated acceleration under a biased electric field, and instantaneous carrier density change in the antenna channel due to the ultrafast pump laser [19,20]. To confirm the generation of the THz radiation (Fig. 1 (b)), the measurement was first carried out using the photoconductor antenna emitter and photoconductive detector. After that, the PA detector was placed to receive the THz beam. A Teflon lens collected the THz beam to the active area of the radiation absorber of the PA detector.

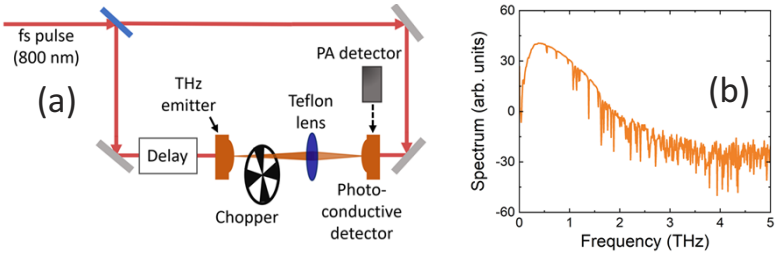

Fig. 1. THz detection process with THz-TDS system: (a) Simplified diagram of THz-TDS setup with 800 nm fs mode-locked Ti: sapphire pump laser to generate THz radiation from the THz emitter. (b) To confirm generation of broadband THz radiation, the output THz spectrum was monitored using a photoconductive detector before the experiments with PA detector.

Figure 2 (a) shows the schematic diagram of the experimental setup at the Physikalisch-Technische Bundesanstalt (PTB, the German National Metrology Institute) [21] for studying the responsivities of CNT absorbers. The output of the molecular gas THz laser was directed by two off-axis parabolic mirrors towards the gold-plated chopper after passing through an aperture. The chopped radiation was focused by a lens into the PA detector which was placed on a precision positioning stage. A reference detector and a THz camera were also mounted on that motor-controlled stage. The gold-plated chopper reflected a part of the THz radiation which was collected by another lens to focus on the monitor detector. The beam profile (Fig. 2 (b)) of 1.4 THz radiation was recorded by the THz camera, at the beginning of the experimental studies. After that, the stage was translated for the reference detector to measure the THz radiation power [22]. Simultaneously, the monitor detector signal was recorded. The process was then repeated for the PA detector to record the corresponding signal. A detailed analysis on spatial scan and responsivity measurements is presented in section 3.

For PA detection, as shown in Fig. 3, the THz radiation chopped at 40 Hz is first absorbed by the absorber material resulting in periodic temperature variation in the PA cell filled with air at the gas pressure of about 1000 hPa. The carrier gas, i.e., air, thus goes through periodic volume expansion and makes the cantilever sensor to exhibit mechanical response due to the generated pressure. The cantilever displacement is finally detected by a built-in interferometer to produce the PA signal. The order of magnitude of the maximum vibration amplitude of the silicon cantilever is 10 μm in regular measurement conditions.

Optics EXPRESS

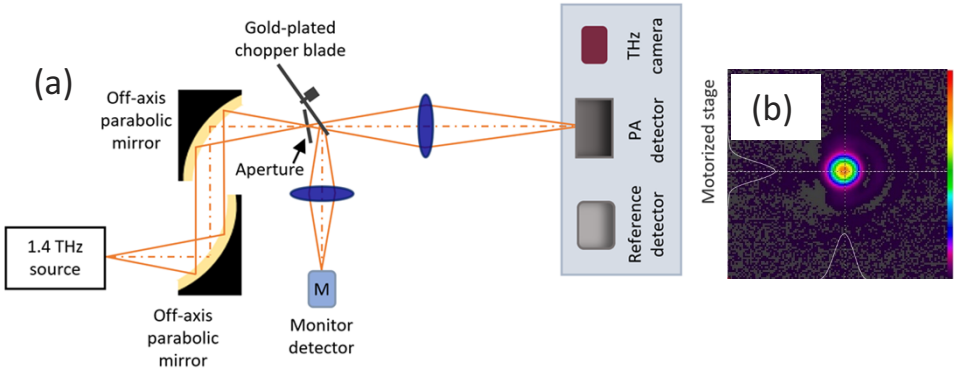

Fig. 2. (a) Schematic diagram of the experimental setup with 1.4 THz source [22] for the responsivity calibration of the PA detector presented in this study. The molecular gas laser at PTB uses CH_2F_2 gas for the generation of 1.4 THz radiation. The THz camera is used for the measurement of the beam profile and the reference detector measures the THz radiation power. (b) Focused beam profile measured with a THz camera (size of image 12.4 × 12.4 mm^2).

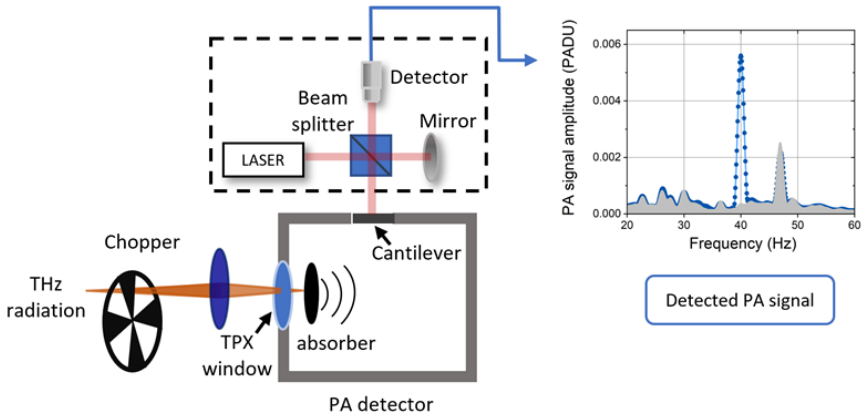

Fig. 3. Simplified diagram of PA detector with radiation absorber which receives the THz radiation chopped at 40 Hz. The mechanical response of the cantilever sensor due to the generated gaseous pressure is detected with an interferometric method to produce the output PA signal.

Optics EXPRESS

3. Experimental results and discussion

The PA response at different chopping frequencies was checked with soot as the absorber material. Figure 4 (a) shows the PA response with broadband THz radiation from the THz-TDS system. As expected, the dependence of responsivity on modulation frequency is similar as reported in [16]. The chopping frequency of 40 Hz was chosen for further studies because it is the same frequency as used in our previous experiments from UV to IR to achieve good signal-to-noise ratio [15–17].

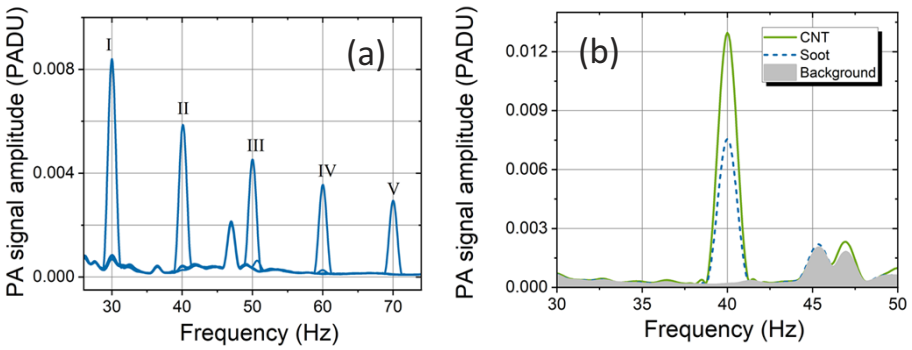

Fig. 4. (a) Dependence of the PA signal on the chopping frequency of THz radiation from THz-TDS system (Fig. 1). The graph depicts separate sequential measurements of the PA signal corresponding to each chopping frequency. The PA signal peaks are numbered by I to V in the graph and the appearance of the 47 Hz peak is possibly due to acoustic vibration of the setup. (b) PA response of soot and CNT absorbers with THz radiation generated at the same pump laser power of the THz-TDS system (Fig. 1).

To compare the absorber materials - soot and CNT, the absorber region was spatially scanned to obtain the highest value of the PA signal amplitude. Figure 4 (b) shows the response of two different absorber materials. The soot material, which showed higher peak amplitude [15,17] from UV to IR region, is found to generate less signal than the CNT when activated with THz radiation of the same power. The results of the experiment show that THz detection is possible with the PA method employing the same cantilever pressure sensor which was used for radiation detection from UV to IR. However, as shown in Fig. 4 (b), we employed CNT as the absorber material for the next experiments at 1.4 THz to obtain better signal amplitude. Previous studies [18,21] have reported absorbers for detector applications in the far IR and THz region. The presented result of our study helped us to select the absorber material to enable PA detection with broad spectral response.

For spatial scanning and responsivity estimation of the PA detector, the laser source at 1.4 THz was employed. Two CNT absorbers, CNT 1 and CNT 2 cut from the same CNT coated plate, were tested. The spatial scan revealed near uniform PA response from the CNT absorbers. Figure 5 (c) and Fig. 5 (d) show photos of absorbers CNT 1 and CNT 2, whereas Fig. 5 (a) and Fig. 5 (b) depict the spatial dependence of the response. The shape of the CNT absorbers can be discerned in the spatial response maps. The PA response is highest around the center of the absorber, but close to the edges of the aluminum sample holder, the response is negligible. It should be noted that it is not easy to obtain as good spatial uniformity with a sensitive Golay cell THz detector due to the structure to optimize the signal strength [13].

The PA response is uniform with THz radiation for both absorbers all over the CNT surface and reduces from 100% to 60% near the absorber edge. Hence, to estimate the responsivity, a region near the central area on the absorber surface was chosen. In the coordinates of Fig. 5, the THz radiation was focused at X = - 1.0 mm and Y = + 0.4 mm for CNT 1, and at X = + 1.9 mm and Y = - 1.0 mm for CNT 2. Figure 6 (a) depicts the PA response of CNT 2 absorber for

Optics EXPRESS

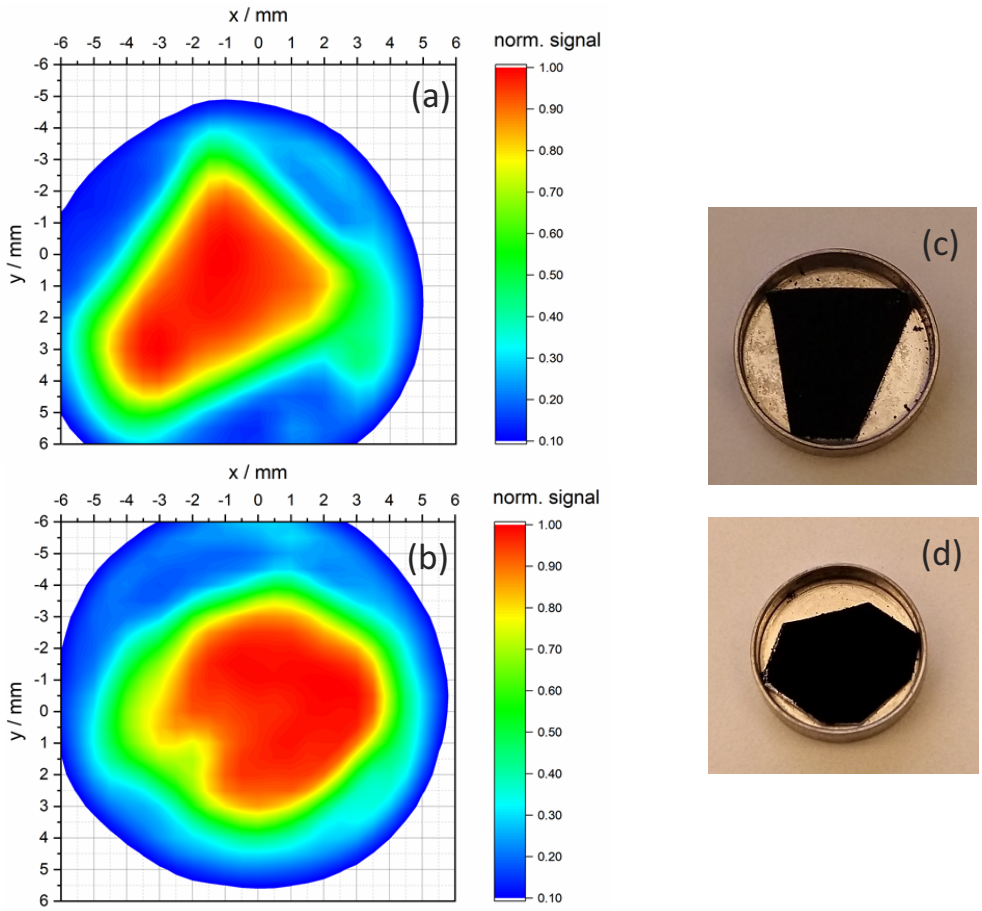

Fig. 5. Two absorbers CNT 1 and CNT 2 were cut from the same CNT coated plate for tests at 1.4 THz (214 µm) with experimental setup presented at Fig. 2 (a). The result of a spatial scan of CNT 1 (a) and of CNT 2 (b), with photos of the actual absorbers, presented in (c) and (d), respectively. The full width at half maximum of the focused Gaussian laser beam at 1.4 THz was 1.9 mm.

Optics EXPRESS

10.47 mW of incident power at 1.4 THz. Figure 6 (b) shows the PA response of both absorbers at different power levels of the incident radiation. The incident power levels of 1.4 THz radiation were measured with THz reference detector at the calibration facility of PTB [21–23]. The responsivity, i.e., the value of the peak amplitude of PA signal per 1 mW of radiation power, can be estimated from the data presented in Fig. 6 (b). The average responsivities of CNT 1 and CNT 2 are 2.04 PADU / mW and 2.06 PADU / mW, respectively, where PADU represents PA detector units. The given units stay fixed if the analog-to-digital conversion process of the PA detector signal is not changed.

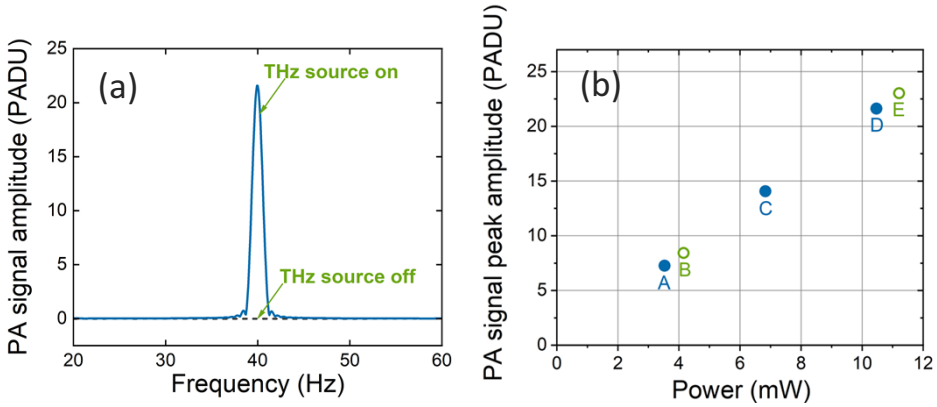

Fig. 6. (a) Demonstration of PA detection of 1.4 THz radiation with CNT 2 absorber. (b) Dependence of peak amplitude of the PA signal on the incident radiation power at 1.4 THz, CNT 1 (green hollow circles) and CNT 2 (blue solid circles). The corresponding responsivity values of CNT 1 as shown by data points B and E are 2.03 PADU / mW and 2.05 PADU / mW, respectively, where PADU represents PA detector units. The responsivities for CNT 2, indicated by data points A, C and D, have the same value of 2.06 PADU / mW.

The PA responsivity of CNT absorbers at 0.633 μm was also measured. Absorbers CNT 1 and CNT 2 showed 13.5 and 14.2 PADU as peak amplitudes of PA signal for 6.1 mW incident radiation power at 0.633 μm wavelength. The optical power at 0.633 μm was measured using a calibrated silicon photodiode detector [16]. The transmittance of the TPX window is dependent on the wavelength. The transmittance is 89.9% at 0.633 μm and 87.3% at 1.4 THz. The correction factor of 1.030 due to the TPX window is applied to values at 1.4 THz (214 μm). Table 1 contains the values of the responsivities of the CNT absorbers for 0.633 μm and 214 μm. The corrected responsivity results of both absorbers agree within 10% at 0.633 μm and 214 μm wavelengths.

Table 1. Comparison of responsivities of CNT absorbers at 0.633 μm and 1.4 THz (i.e., 214 μm wavelength)

Radiation absorbers	Responsivity (PADU / mW) at 0.633 μm	Responsivity (PADU / mW) at 1.4 THz	Corrected responsivity due to TPX window (PADU / mW) at 1.4 THz
CNT 1	2.21	2.04	2.10
CNT 2	2.33	2.06	2.12

The lowest detectable THz power of the PA detector with CNT as absorber material is expected not to be as low as in the case of candle soot absorber in the visible wavelength range [15] because of a factor three lower responsivity and higher ambient vibration level in the laboratory rooms with THz sources. The noise-equivalent power (NEP) is 160 nW/ $\sqrt{\text{Hz}}$ with almost five orders of magnitude demonstrated dynamic range of PA detection of THz radiation. The estimated

Optics EXPRESS

NEP is the ratio of P_σ to the square root of the measurement bandwidth (1.3 Hz), where P_σ is the power corresponding to the signal-to-noise ratio of value 1. Power P_σ was calculated using the responsivity of the absorber and the root-mean-square value of the background noise at the modulation frequency.

In Fig. 6 (b), we have no data between the lowest detectable power and 3 mW, but the response should be linear because the PA detector shows linear response in the UV-IR wavelength range [16,17]. The PA detection process is exactly similar in the UV-IR region and in THz range after conversion of the electromagnetic radiation to heat. The used power range in measurements at 1.4 THz and the NEP are limited by the available radiation source and ambient vibration level, respectively, which indicate a potential for a larger dynamic range in applications where such extension is needed.

4. Conclusion

We have presented a PA detection method which can be applied to measure electromagnetic radiation power of both visible and THz radiation. In measurements with the THz-TDS system as the radiation source, CNT absorber material showed better signal peak amplitude than soot absorber. In addition, a spatial scan at 214 μm wavelength (1.4 THz) depicts a nearly uniform PA response in most of the area around the central region of the CNT surface, which is an advantage as compared with sensitive Golay cell detectors. Other advantages of the PA detector are large dynamic range and high damage threshold for unintentionally coupled intense THz radiation. For the latter, it can be estimated that a cantilever displacement of more than 1 mm is needed to damage the sensor. Cantilever vibration amplitudes in regular measurements are two orders of magnitude smaller.

Previously reported results [17] show that the PA responsivity with CNT absorber is approximately constant between 0.3 μm and 15 μm wavelengths, including measurements at 0.633 μm. The results of the present work suggest that the PA responsivity of the CNT material is approximately constant up to 214 μm wavelength. However, to fully utilize the absorber property, the window of the detector should have transmittance over the whole wavelength range i.e., UV to THz. The PA detection method presented in this study, has the potential to serve as a single detection unit for power measurement applications to cover a significantly broad spectral range including visible and THz with large dynamic range and high damage threshold of the sensor.

Funding. Academy of Finland (320167, 314364, 326444).

Acknowledgments. We thank Gasera Ltd. for designing the commercially available instrument parts employed in the experiments.

Disclosures. The authors declare no conflicts of interest.

Data availability. Data underlying the results presented in this paper are not publicly available at this time but may be obtained from the authors upon reasonable request.

References

1. R. A. Lewis, "A review of terahertz detectors," J. Phys. D: Appl. Phys. **52**(43), 433001 (2019).
2. JS. Rieh, *Introduction to Terahertz Electronics* (Springer, 2021, Chap. 3).
3. F. Sizov and A. Rogalski, "THz detectors," Prog. Quantum Electron. **34**(5), 278–347 (2010).
4. S. S. Dhillon, M. S. Vitiello, E. H. Linfield, A. G. Davies, M. C. Hoffmann, J. Booske, C. Paoloni, M. Gensch, P. Weightman, G. P. Williams, E. Castro-Camus, D. R. S. Cumming, F. Simoens, I. Escorcia-Carranza, J. Grant, S. Lucyszyn, M. Kuwata-Gonokami, K. Konishi, M. Koch, C. A. Schmuttenmaer, T. L. Cocker, R. Huber, A. G. Markelz, Z. D. Taylor, V. P. Wallace, J. A. Zeitler, J. Sibik, T. M. Korter, B. Ellison, S. Rea, P. Goldsmith, K. B. Cooper, R. Appleby, D. Pardo, P. G. Huggard, V. Krozer, H. Shams, M. Fice, C. Renaud, A. Seeds, A. Stöhr, M. Naftaly, N. Ridler, R. Clarke, J. E. Cunningham, and M. B. Johnston, "The 2017 terahertz science and technology roadmap," J. Phys. D: Appl. Phys. **50**(4), 043001 (2017).
5. N. Laman, S. S. Harsha, D. Grischkowsky, and J. S. Melinger, "7 GHz resolution waveguide THz spectroscopy of explosives related solids showing new features," Opt. Express **16**(6), 4094–4105 (2008).
6. D. Molter, J. Klier, S. Weber, M. Kolano, J. Jonuscheit, and G. von Freymann, "Two decades of terahertz cross-correlation spectroscopy," Appl. Phys. Rev. **8**(2), 021311 (2021).

Optics EXPRESS

7. J. F. Federici, B. Schulkin, F. Huang, D. Gary, R. Barat, F. Oliveira, and D. Zimdars, "THz imaging and sensing for security applications-explosives, weapons and drugs," Semicond. Sci. Technol. **20**(7), S266–S280 (2005).
8. Y. Takida, K. Nawata, S. Suzuki, M. Asada, and H. Minamide, "Nonlinear optical detection of terahertz-wave radiation from resonant tunneling diodes," Opt. Express **25**(5), 5389–5396 (2017).
9. A. E. Yachmenev, R. A. Khabibullin, and D. S. Ponomarev, "Recent advances in THz detectors based on semiconductor structures with quantum confinement: a review," J. Phys. D: Appl. Phys. **55**(19), 193001 (2022).
10. C. Belacel, Y. Todorov, S. Barbieri, D. Gacemi, I. Favero, and C. Sirtori, "Optomechanical terahertz detection with single meta-atom resonator," Nat. Commun. **8**(1), 1578 (2017).
11. N. Glauvitz, R. A. Coutu, I. R. Medvedev, and D. T. Petkie, *Progresses in Chemical Sensor* (IntechOpen, 2016, Chap. 2).
12. N. E. Glauvitz, R. A. Coutu, I. R. Medvedev, and D. T. Petkie, "Terahertz Photoacoustic Spectroscopy Using an MEMS Cantilever Sensor," J. Microelectromech. Syst. **24**(1), 216–223 (2015).
13. Tydex https://www.tydexoptics.com/ accessed on 19 August 2022.
14. Microtech Instruments www.mtinstruments.com accessed on 19 August 2022.
15. J. Rossi, J. Uotila, S. Sharma, T. Laurila, R. Teissier, A. Baranov, E. Ikonen, and M. Vainio, "Photoacoustic characteristics of carbon-based infrared absorbers," Photoacoustics **23**, 100265 (2021).
16. S. Sharma, T. Laurila, J. Rossi, J. Uotila, M. Vainio, F. Manoocheri, and E. Ikonen, "Electromagnetic radiation detection using cantilever-based photoacoustic effect: A method for realizing power detectors with broad spectral sensitivity and large dynamic range," Sens. Actuators, A **337**, 113191 (2022).
17. J. Rossi, J. Uotila, S. Sharma, T. Hieta, T. Laurila, R. Teissier, A. Baranov, E. Ikonen, and M. Vainio, "Optical power detector with broad spectral coverage, high detectivity, and large dynamic range," Opt. Lett. **47**(7), 1689–1692 (2022).
18. J. H. Lehman, B. Lee, and E. N. Grossman, "Far infrared thermal detectors for laser radiometry using a carbon nanotube array," Appl. Opt. **50**(21), 4099–4104 (2011).
19. P-I Lin, S-F Chen, K-H Wu, J-Y Juang, T-M Uen, and Y-S Gou, "Characteristics of Photogenerated Bipolar Terahertz Radiation in Biased Photoconductive Switches," Jpn. J. Appl. Phys. **41**(Part 2, No. 10B), L1158–L1160 (2002).
20. S. Verghese, K. A. McIntosh, and E. R. Brown, "Optical and terahertz power limits in the low-temperature-grown GaAs photomixers," Appl. Phys. Lett. **71**(19), 2743–2745 (1997).
21. R. Müller, W. Bohmeyer, M. Kehrt, K. Lange, C. Monte, and A. Steiger, "Novel detectors for traceable THz power measurements," J Infrared Milli Terahz Waves **35**(8), 659–670 (2014).
22. A. Steiger, M. Kehrt, C. Monte, and R. Müller, "Traceable terahertz power measurement from 1 THz to 5 THz," Opt. Express **21**(12), 14466–14473 (2013).
23. B. Globisch, R. J. B. Dietz, T. Göbel, M. Schell, W. Bohmeyer, R. Müller, and A. Steiger, "Absolute terahertz power measurement of a time-domain spectroscopy system," Opt. Lett. **40**(15), 3544–3547 (2015).